nature communications



Article

https://doi.org/10.1038/s41467-025-59631-3

Structural reconfiguration of interacting multi-particle systems through parametric pumping

Received: 9 October 2024

Qingnao Mao u

Qinghao Mao ^{1,2} ⋈, Brady Wu^{1,2}, Bryan VanSaders² & Heinrich M. Jaeger ^{1,2}

Accepted: 25 April 2025

Published online: 19 May 2025

Check for updates

Processes from crystallization to protein folding to micro-robot self-assembly rely on achieving specific configurations of microscopic objects with short-ranged interactions. However, the small scales and large configuration spaces of such multi-body systems render targeted control challenging. Inspired by optical pumping manipulation of quantum states, we develop a method using parametric pumping to selectively excite and destroy undesired structures to populate the targeted one. This method does not rely on free energy considerations and therefore works for systems with non-conservative and even non-reciprocal interactions, which we demonstrate with an acoustically levitated five-particle system in the Rayleigh limit. With results from experiments and simulations on three additional systems ranging up to hundreds of particles, we show the generality of this method, offering a new path for non-invasive manipulation of strongly interacting multi-particle systems.

Precise control of multi-particle systems is challenging due to the multiplicity of stable structures within a high-dimensional configuration space. To guide such systems towards the targeted structure, techniques such as acoustic¹⁻⁴ or optical trapping⁵⁻⁸ create localized field gradients that apply forces on individual particles. This has enjoyed success for facile particle manipulation with wide-ranging applications, including reconfigurable displays and phononic crystals⁹⁻¹¹. However, these methods isolate particles into potential wells that are separated on the scale of the incident wavelength, preventing their applicability to structures with closely spaced particles where particle interactions become important. Another approach, therefore, focuses on utilizing the particle interactions themselves to tailor the free-energy landscape. This creates an effective guiding force favoring the desired configuration, employing methods based on, e.g., electromagnetic interactions¹²⁻¹⁶, shaped and patchy particles¹⁷⁻¹⁹, or DNA bonding^{20–22}. These methods are typically optimized to produce a single targeted configuration and cannot be extended easily to allow for reconfigurability. Out-of-equilibrium self-assembly²³⁻²⁵ further complicates this picture by invalidating the basic notion of a uniquely defined free-energy landscape, and consequentially the precise control of such systems remains difficult. These shortcomings can be somewhat alleviated using active feedback control to apply corrective forces^{14,25,26}, at the cost of requiring real-time sensing, actuation, and substantial computation. Still, structural control remains a non-trivial task, even for clusters containing only a small number of particles^{27–31}. This can be yet more complicated in non-conservative systems with non-reciprocal interactions^{32–34}.

To address this problem, we borrow an idea from optical pumping³⁵. Consider a two-state system (Fig. 1a), where incident light pumps state A into an unstable excited state before it randomly decays into either state A or B. Due to the mismatch of gap energy, B is an absorbing state that cannot be activated, so the concentration of state B grows as the excitation and decay of A continues. Thus, precise state control is achieved without a feedback loop by selectively activating and depopulating the undesired states. We can adapt this strategy for precise assembly of particles in many systems with tunable interactions^{4,7,36-39}, including those without energy conservation, provided that the states to be manipulated are not isospectral^{40,41}, i.e., that these states have distinguishable vibrational bands. Specifically, we use parametric pumping⁴²⁻⁴⁴ to excite and destabilize undesired structures, combined with quenching to favor the targeted one, as sketched in Fig. 1b. By cycling between pumping and quenching, we effectively

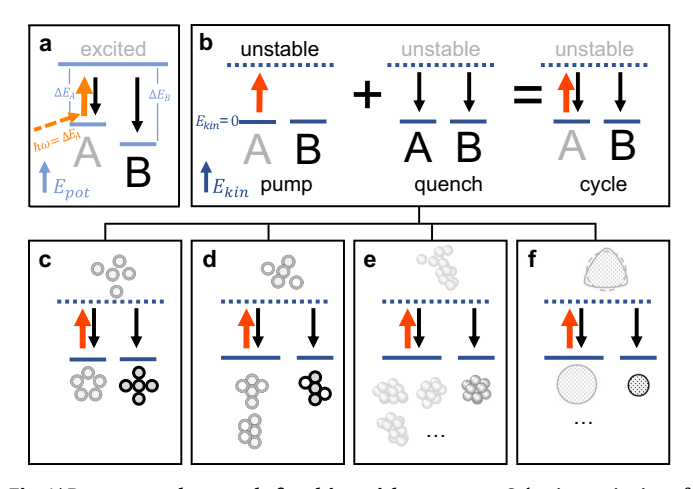


Fig. 1 | Pump-quench control of multi-particle systems. a Selective excitation of state A in a system of trapped atoms, creating a dark state B. The vertical axis indicates the potential energy of the system, E_{pot} . When state A is excited by light with appropriate energy, it will be pumped into an excited state (orange arrow), from which it can randomly decay into one of the base states (black arrows). State B cannot be activated by incident light; thus, pumping concentrates atoms in state B. **b** Cycling between pumping and quenching to create an absorbing 'quiet' state, which does not rely on the presence of well-defined potential energy levels and therefore is not limited to conservative systems. The vertical axis indicates the kinetic energy, E_{kin} , where E_{kin} = 0 refers to a base state of the system. By activating a multi-particle system's vibration mode with parametric pumping, the system will oscillate to the point of transitioning into an unstable state (red arrow). When the pumping is turned off, the system in the unstable state is quenched by damping and will randomly decay back into one of the base states. By cycling between pumping and quenching, the time-averaged outcome is the creation of an absorbing state B, similar to the diagram in (a). c-f Application of pump-quench cycling to control the configuration of, c an acoustically levitated cluster of five particles, d a simulated cluster of a rod and two spheres, e a simulated cluster of 13 spheres, and f the size of an acoustically levitated granular raft.

create a diagram similar to Fig. 1a, where state B is 'quiet' and absorbing. This method reduces the high-dimensional control problem to a 1D frequency domain and, simultaneously, circumvents the need to fine-tune energy landscapes for state selection, enabling us to control systems with non-reciprocal interactions as well.

In the following, we demonstrate this approach with experiments and simulations that focus on acoustically levitated particle systems. We first discuss a five-particle system with non-reciprocal interactions, Fig. 1c, showing reversible control between two configurations. We then extend the method to systems with a larger number of excitable configurations from which we can select targeted outcomes: a cluster of levitated particles with anisotropic shape, Fig. 1d; a 3D Lennard-Jones cluster of 13 particles, Fig. 1e; and a levitated granular raft comprising hundreds of particles, Fig. 1f.

Results

Acoustic levitation system

We use a single-axis Langevin-type horn to generate intense ultrasound (frequency $f \approx 34,800\,\mathrm{Hz}$) capable of lifting small particles against the force of gravity, as shown in Fig. 2a. A piezoelectric transducer driven by a function generator is affixed to an aluminum horn, which acts as a resonant amplifier. The horn is positioned one half wavelength ($h = \lambda/2$) above a transparent reflector plate, creating a standing sound wave. Particles levitate just below the pressure nodal plane, midway in the gap. The bottom surface of the resonant horn is slightly curved, which focuses the sound and also produces lateral confinement of particles near the center of the nodal plane. We use polystyrene spheres with diameter $D = 41\,\mu\mathrm{m}$. Residual charge on particle surfaces is eliminated by a photo-ionizer, and the reflector

plate is ITO-coated and grounded. Two high-speed cameras capture simultaneously the side and the bottom view of levitated particles. A pressure sensor is positioned near the acoustic cavity to measure and control the acoustic pressure. Details about the acoustic levitation setup are discussed in Methods.

Parametric pumping in a two-particle system

We first demonstrate acoustic parametric pumping of a 'molecule' consisting of two spheres mutually bound by sound-induced forces. In this simplest case, the interaction is conservative and (to linear order) spring-like. For two solid, levitating spheres with diameters and center-to-center distance r much smaller than the wavelength of incident sound (the near-field Rayleigh limit, $\lambda \gg r \geq D$), the net force at close approach arises from the competition between attractive acoustic scattering force and repulsive force from viscous streaming flow near the particle boundaries³⁴.

As sketched in Fig. 2b, the balance between the two forces results in a stable, steady-state separation r_{ss} of the two particles in the 'molecule'. Importantly, both forces are proportional to the sound energy density E in the acoustic cavity. Therefore, r_{ss} does not change when E is tuned by a changing sound pressure. However, the effective spring constant for small displacements around r_{ss} does scale with E, as shown in Fig. 2c. This enables us to selectively excite internal degrees of freedom of interacting particles with parametric pumping, which is fundamentally different from modulating a background field to move particles collectively^{1,3,44}. More detailed discussion of the scattering and streaming interactions can be found in refs. 4,34.

To conduct parametric pumping, we modulate transducer input voltage by varying the amplitude according to $(1+\varepsilon_{am}\sin(2\pi f_{am}t))$, where f_{am} is the modulation frequency and ε_{am} the modulation depth, Fig. 2d. Since energy density E depends quadratically on transducer voltage³⁴, it becomes

$$E = E_0 (1 + \varepsilon_{\text{am}} \sin(2\pi f_{\text{am}} t))^2. \tag{1}$$

When levitated particles are subject to such a modulated acoustic field, tuning $f_{\rm am}$ and $\varepsilon_{\rm am}$ can activate specific vibrational modes (VMs), growing their vibration amplitude to destabilize the structure. As an example, the pumping state diagram in Fig. 2e shows how the effective growth rate of the in-plane 'breathing' mode of the two-particle system, $\gamma_2^* = \frac{\gamma_2}{\gamma_d}$ ' depends on both $f_{\rm am}$ and $\varepsilon_{\rm am}$. Here γ_2 is the growth rate without damping, and γ_d is the damping rate caused by air viscosity, see Methods. See Supplementary Information for out-of-plane VMs. Similar to solutions of Mathieu's equation⁴⁵, we find that the VM can be activated within Arnold tongues, i.e., with sufficiently large $\varepsilon_{\rm am}$ when $f_{\rm am}$ is close to a factor 2/n times the VM's resonance frequency ($n \in Z+$). The isolines $\gamma_2^* = 1$, where growth rate equals damping rate, are shown as gray lines in Fig. 2e. Only regions that have $\gamma_2^* > 1$ can be used to pump a VM.

Because the acoustic cavity has a finite response time and also a characteristic response function that depends on f, $f_{\rm am}$ and $\varepsilon_{\rm am}$, the experimentally measured, steady-state modulation depth in the acoustic trap, $\varepsilon_{\rm am}^{\rm eff}$, is usually smaller than $\varepsilon_{\rm am}$. Therefore, when analyzing VMs and comparing with simulations, we need to consider $\varepsilon_{\rm am}^{\rm eff}$. The largest $\varepsilon_{\rm am}^{\rm eff}$ achievable in our setup, i.e., using 100% piezo voltage modulation at different frequencies, is shown in Fig. 2e. If the system is driven with f= 34,650 Hz (pink), away from the cavity resonance $f_{\rm res}$ = 34800Hz (red), a higher $\varepsilon_{\rm am}^{\rm eff}$ can be achieved(see Supplementary Information), crossing the γ_2^* = 1 isolines and allowing for VM pumping.

In Fig. 2f, we show two snapshots of the pumped 2-sphere system, and in Fig. 2g, we plot their center-to-center distance r(t) as a function of time, demonstrating how parametric pumping activates this inplane VM (also see Supplementary Movie 1). Vibration amplitude saturates at larger t because the pumping rate γ_2 drops and γ_d grows as the system departs the linear region, yielding $\gamma_2^* = 1$.

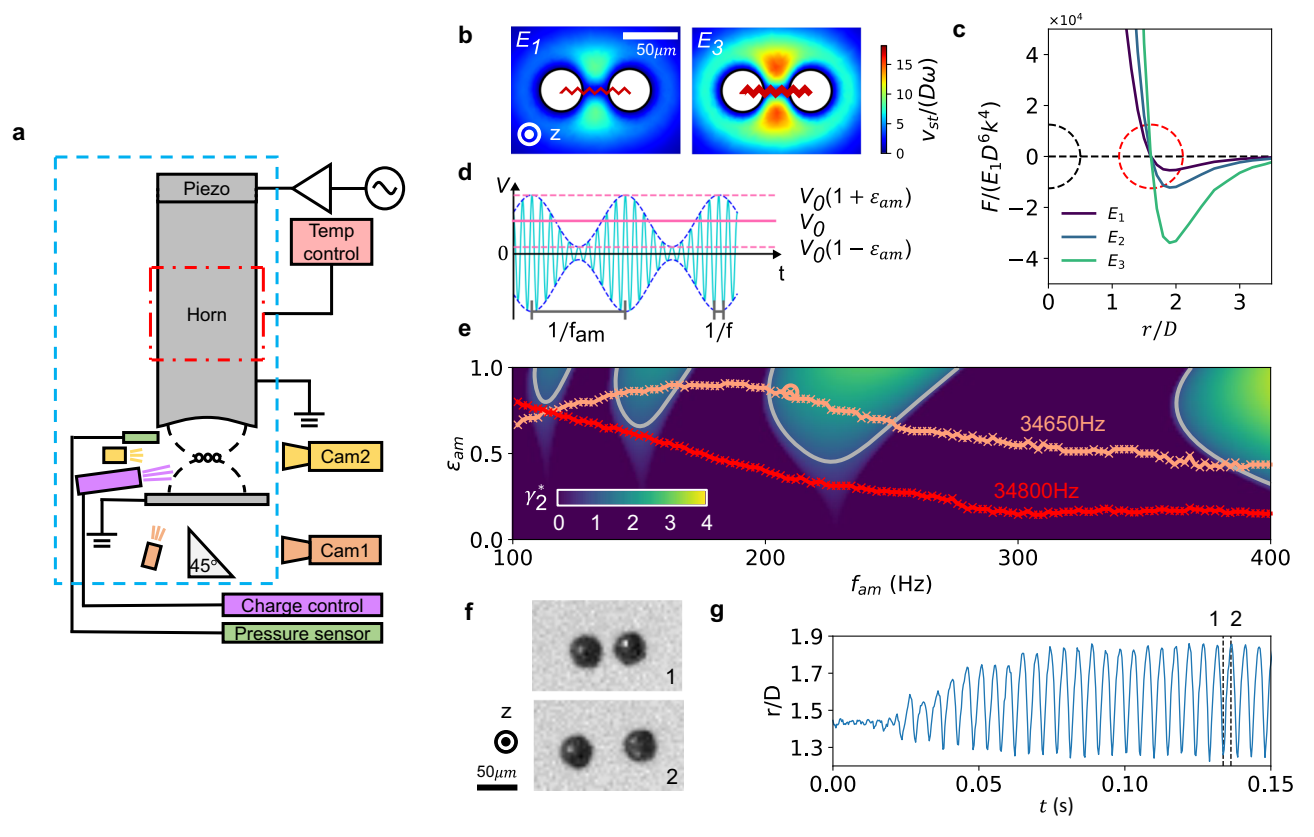


Fig. 2 | **Acoustic parametric pumping. a** Diagram of experimental setup. **b** Tunable acoustic interactions between particles. The right plot has a higher acoustic power than the left. The thickness of the red lines connecting the particle centers indicates the strength of the effective spring constant and the background shows the streaming flow velocity field magnitude v_{st} , from finite-element method simulation. **c** Sound-induced net force between two spheres, for acoustic energy densities $E_1 < E_2 < E_3$. **d** Piezo input voltage with modulating frequency f_{am} and

modulation depth ε_{am} , **e** Pumping state diagram for the in-plane vibration mode of the 2-sphere `molecule', showing the mode's growth rate γ_2^* as function of f_{am} and ε_{am} . Gray isolines indicate $\gamma_2^* = 1$, where pumping balances dissipation. Maximum modulation depth in the experiments at two sound frequencies is shown by red and pink lines. **f** Video snapshots of a 2-sphere 'molecule' pumped with parameters marked by the pink circle in (**e**). **g** Center-to-center distance r between two spheres when pumped. Dashed vertical lines refer to the snapshots in (**f**).

Adding complexity: multibody and non-reciprocal interactions

Adding particles increases the variety of possible stable configurations in the levitation plane. For five levitating spheres, the interactions due to attractive sound scattering and repulsive microstreaming allow for two such configurations: either a pentagon or a cross structure, as shown in Fig. 3a. Furthermore, while the interactions between a pair of levitated spheres can be well-approximated with a pair potential of levitated spheres can be well-approximated with a pair potential of levitated spheres can be well-approximated with a pair potential of levitated spheres can be well-approximated with a pair potential of levitated spheres can be well-approximated with a pair potential of levitated spheres can be well-approximated with a pair potential of levitated spheres can be well-approximated with a pair potential of levitated spheres can be well-approximated with a pair potential of levitated spheres can be well-approximated with a pair potential of levitated spheres can be well-approximated with a pair potential of levitated spheres can be well-approximated with a pair potential of levitated spheres can be well-approximated with a pair potential of levitated spheres can be well-approximated with a pair potential of levitated spheres can be well-approximated with a pair potential of levitated spheres can be well-approximated with a pair potential of levitated spheres can be well-approximated with a pair potential of levitated spheres can be well-approximated with a pair potential of levitated spheres can be well-approximated with a pair potential of levitated spheres can be well-approximated with a pair potential of levitated spheres can be well-approximated with a pair potential of levitated spheres can be well-approximated with a pair potential of levitated spheres can be well-approximated with a pair potential of levitated spheres can be well-approximated with a pair potential of levitated spheres can be well-approximated with a pair potential of levitated spheres can be well-approximated with a pair p

We now focus on a pair of particles (indicated by the pink dashed line that links their centers), where one particle is displaced 0.3*D* to the left or right of its stable position. In both cases, resulting force felt by the other one (red arrow) are not pointing along the pink dashed line, nor pointing in the same direction. This is not possible for pairwise interactions, rather signaling multibody interactions that arise from background flow field generated by all particles collectively.

The sound-induced interactions also violate Newton's third law, i.e., the force on particle A due to the presence of particle B is not equal and opposite to the force on B due to A. This non-reciprocity can be detected as an asymmetry in the linear stiffness matrix describing the five-particle system (Supplementary Fig. 2). The multibody and non-reciprocal nature of the levitated 5-particle system implies that we cannot define a unique energy landscape connecting both structures, rendering it infeasible for a landscape tuning method to drive this system between configurations. However, this is possible with parametric pumping, as discussed next.

Reversible shape-shifting with a 5-particle cluster

Irrespective of the complexity of the interactions among particles, to linear order, we can obtain the VMs and their associated eigenfrequencies from the stiffness matrix for each stable configuration. By diagonalizing the stiffness matrices calculated by FEM simulation, we find 8 VMs for the cross state and 6 for the pentagon state (Supplementary Fig. 3). We then calculate the effective growth rates $\gamma_{[c,p],i}^*(f_{
m am}, \varepsilon_{
m am})$ for all i modes of the cross (c), and pentagon (p) states in the same way as for the two-particle system. The maximum of these growth rates for a given state, $\gamma_{[c,p]}^*(f_{am}, \varepsilon_{am}) = \max_i(\gamma_{[c,p],i}^*(f_{am}, \varepsilon_{am}))$ is shown in blue and red for the cross and the pentagon, respectively, in the pumping state diagram in Fig. 3d. We can find combinations of $(f_{\rm am}, \varepsilon_{\rm am})$ that activate one (blue or red), both (purple) or none (white) of the states. Note that only the region on and below $\varepsilon_{\mathrm{am}}^{\mathrm{eff}}(f_{\mathrm{am}})$, shown by the black line, is accessible to us experimentally with f = 34,750 Hz. On that line, two locations suitable for parametric pumping are marked by the blue cross and red pentagon symbol.

Figure 3e and Supplementary Movie 1 give an example of guiding the five-particle cluster to form a cross. The sound field is driven with $f_{\rm am}$ = 290 Hz, $\varepsilon_{\rm am}^{\rm eff}$ = 0.40 (red pentagon symbol in Fig. 3d) to destabilize the pentagon without affecting the cross. As a result, during the first pumping cycle the cluster is excited into the unstable state and during quenching (e.g., when the sound field modulation is turned off) it relaxes back into the pentagon state. The second pumping cycle drives the cluster unstable again, but this time it relaxes into the cross state during quenching, where it remains in subsequent cycles. The opposite transition can also be achieved, as shown in Fig. 3f and

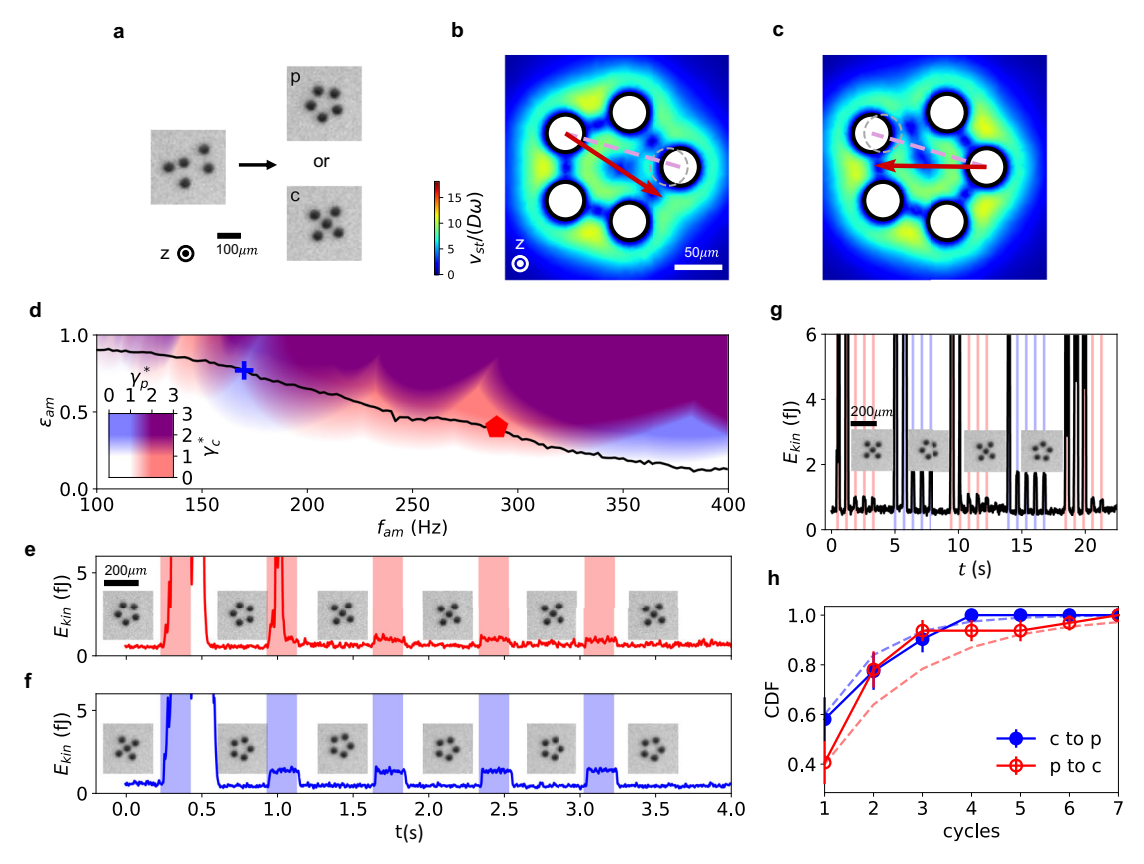


Fig. 3 | **Reversible reconfiguration of a levitated 5-sphere cluster with non-reciprocal interactions. a** Snapshot of five spheres in the unstable state (left) and in their two stable states, pentagon and cross (right). **b**, **c** Simulation of steady streaming flow velocity field magnitude v_{st} around the five spheres when one sphere is displaced by 0.3D (original position indicated by gray dashed circle). Red arrows show the net force felt by the sphere at the other end of the dashed pink lines. **d** Overlay of pumping state diagrams for the cross state, γ_c^* (blue) and the pentagon state, γ_p^* (red). The maximum modulation depth in the experiment is indicated by the black line. Pumping parameter combinations marked by the blue

cross and the red pentagon are chosen to activate one or the other state.

e, f Transitioning between states. Plots show total kinetic energy when the pentagon, or the cross state, is repeatedly pumped (time intervals shaded light red or blue) and quenched (white), with snapshots of the evolving configurations.

g Reversible switching between cross and pentagon states by altering the pumping parameters on the fly. h Cumulative probability of successful transitioning as a function of cycles needed. Solid lines: experiments; dashed lines: Markov model. Error bars: standard deviation.

Supplementary Movie 1, where the sound field is modulated using $f_{\text{am}} = 170 \text{ Hz}$, $\varepsilon_{\text{eff}}^{\text{eff}} = 0.77$ (blue cross symbol in Fig. 3d).

The pumping parameters $f_{\rm am}$ and $\varepsilon_{\rm am}$ can be adjusted on the fly, giving the flexibility of switching rapidly back and forth between the two configurations of the 5-particle cluster. This is demonstrated in Fig. 3g and Supplementary Movie 1. For both directions, only a few pump-quench cycles are required for a high probability of configuration switching (Fig. 3h). This agrees qualitatively with a Markov model of the pump-quench process (dashed lines, see Methods).

Particle systems with more complicated configuration space

To show how the pump-quench approach performs in scenarios where the configuration space is more complicated than for the 5-sphere system, we next discuss simulations of a particle cluster with three states and a cluster with over 70 states. The first example consists of two spheres interacting with a rigid rod comprised of three spheres, as shown in the inset of Fig. 4a. Forces between particles are designed to mimic the conservative-part of interactions in the experiment(see Methods) and this system has three stable configurations(inset: red, green and blue) with similar energies.

In the simulation, we can modulate the interaction strength between particles directly (rather than indirectly via the energy density, Eq. (1)). Thus, the effective spring constant is modulated according to $k = k_0(1 + \varepsilon_{\rm am} \sin(2\pi f_{\rm am}t))$. The pumping state diagram of this system is shown in Fig. 4a. Again, we can find pumping parameter

combinations where only one state is activated (red, green, and blue), two states are activated simultaneously (pink, cyan, and gold), or all three states are activated (black). With these parameter combinations, we can design pump-quench sequences that guide the system into different targeted configurations.

For example, if the blue configuration is targeted as the desired end state, the red and the green ones have to be activated and destabilized. To achieve this, we can first pump with parameters marked by the red cross and activate the red structure, then quench and next use the parameters marked by the green cross to activate the green structure, then quench again. Repeating this particular sequence makes the blue state absorbing. Starting from 1000 random initial conditions, the blue squares in Fig. 4b show that the probability of not attaining the blue structure decreases exponentially with the number of quenching steps. This matches the prediction from a Markov model (the dashed line, see Methods). The same applies when instead the red or the green structure is targeted.

Because there are regions in the pumping state diagram where multiple states can be activated simultaneously, we can implement a second method where we destabilize two structures at the same time using parameters marked by the circles in Fig. 4a. This is significantly more efficient (Fig. 4b circles), as confirmed by the shorter absorbing time calculated from the Markov models (Supplementary Fig. 4).

The second example is a three-dimensional cluster of 13 particles with Lennard-Jones interactions. Simulating this system at zero

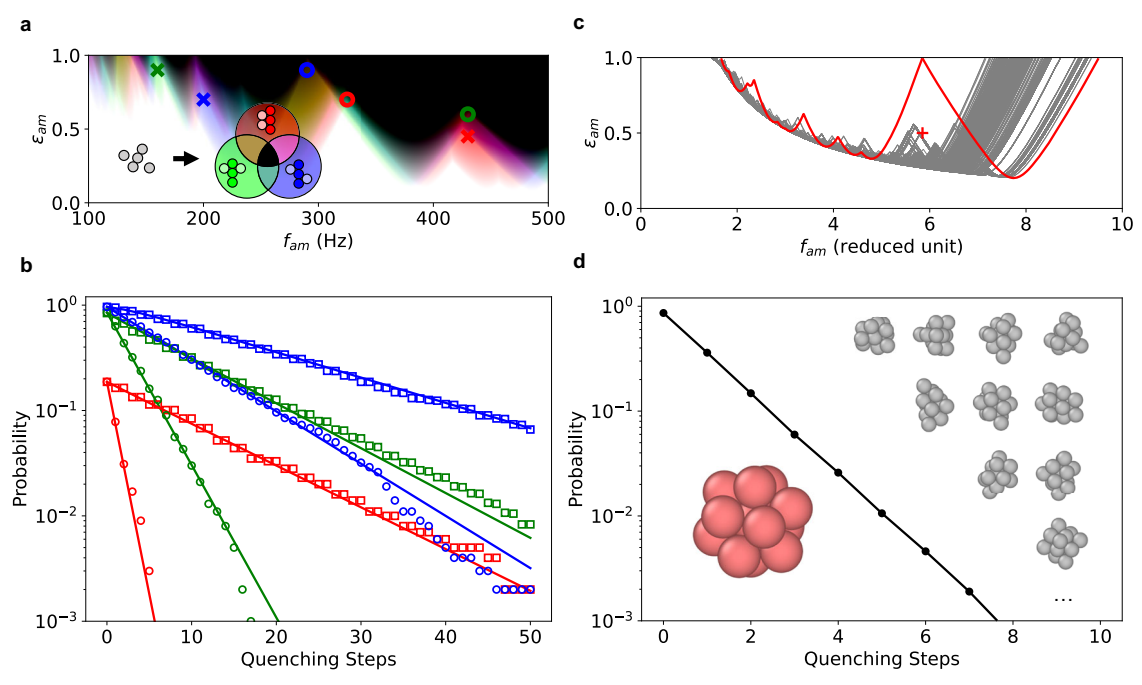


Fig. 4 | **Extension to systems with more complicated configuration space. a** Pumping state diagram for a simulated 3-state system comprising a rod and two spheres. Inset: color code for the particle configurations corresponding to the three states and their activation. At certain spots in the state diagram, only one state is activated (red, blue, and green) or one state is stable (pink, cyan, and gold), or all three states are activated (black). **b** Probability of not reaching the targeted state decreases exponentially. Protocol I (square symbols) applies pump-quench cycles alternating between two sets of parameters marked by crosses with different colors in **a**. Protocol II (circle symbols) applies a single-step process using parameters marked by the circles in **a**. Open symbols: simulation data. Color of the circle

symbol denotes the targeted structure. Lines: Markov model. $\bf c$ Pumping state diagram for a simulated cluster of 13 spheres with Lennard-Jones interactions at T=0. In this three-dimensional cluster all spheres are in direct contact with neighbors. Red line shows the boundary above which pumping is possible $(\dot{\bf y'}=1)$ for the icosahedral sphere arrangement; gray lines are the boundaries for other structures. Red cross: the specific pumping parameter combination used. $\bf d$ Probability of not reaching the targeted icosahedral configuration (sketched in red) decreases exponentially. Examples of other, non-targeted configurations are sketched in gray.

temperature, we find >70 distinct stable structures. This leads to a pumping state diagram densely populated with overlapping resonant regions (Fig. 4c), each corresponding to combinations of parameters ε_{am} and f_{am} that activate a particular configuration, some of which are shown in gray in Fig. 4d. However, there still are non-overlapping regions that allow for certain configurations to be selected. Here we show this for the icosahedral configuration (red in Fig. 4d), whose activation boundary in the pumping state diagram in Fig. 4c is indicated by the red line. Due to the high symmetry of the icosahedron, its activation region exhibits a characteristic gap as a function of f_{am} , which allows us to destabilize all other structures by pumping with parameters marked by the red (+) sign. Similar to the previous example, when starting from 10⁴ random initial states, the probability of not reaching the targeted icosahedron decays exponentially with the number of pump-quench cycles (Fig. 4d). While the clear gap in the spectrum of vibration frequencies makes the icosahedral configuration particularly selectable, configurations with more overlap in the state diagram can be targeted similarly. We show this in the Supplementary Information, where we discuss how structural symmetry, damping coefficient, particle number, and number of states affect state selectability.

Application to bulk vibration modes

As the particle number increases, the pumping state diagram becomes more crowded, and it becomes more difficult to selectively activate individual configurations or find absorbing states. Nevertheless, parametric pumping can still be utilized to activate collective, bulk vibration modes. Here we show how this can be employed to control the size of a levitated granular raft containing more than 300 particles. Rafts of this size can be driven to exhibit bulk oscillations in their

overall shape, similar to levitated liquid drops⁴². With our experimental setup, the frequencies most conveniently accessible to destabilize the raft belong to the shape oscillation mode with threefold symmetry. As shown in Fig. 5a and Supplementary Movie 2, by pumping this mode for 0.3 s, the raft as a whole is excited so strongly that particles no longer stay bound acoustically and escape. When subsequently quenched for 1s, the raft stabilizes, but at a reduced size due to loss of particles. Rafts of different sizes and therefore different masses exhibit shape oscillation resonances centered around different frequencies, similar to liquid droplets where these resonances are given by Rayleigh's equation⁴². Therefore, when the pump-quench cycling is continued with fixed f_{am} , the raft's size will eventually become too small to be activated and will no longer lose particles. Thus, by starting with large rafts and applying different pumping frequencies f_{am} , different terminal raft sizes can be targeted (Supplementary Fig. 8). Figure 5b shows how this self-limiting process shrinks large rafts. The raft size saturates automatically over 20 pump-quench cycles as the targeted diameter is approached. On the right, initial and final images of the rafts are compared, with color corresponding to the data for different f_{am} .

Discussion

Our results show that cyclic switching between parametric pumping and quenching can control the structural configuration of strongly interacting particle systems even when the interactions are multibody and non-reciprocal in nature. Instead of engineering highly localized potential gradients, this approach excites vibrational modes to drive the (re-) configuration process. As such, our method does not rely on an underlying free-energy landscape and thus can work with nonconservative systems. It does not depend on specific particle

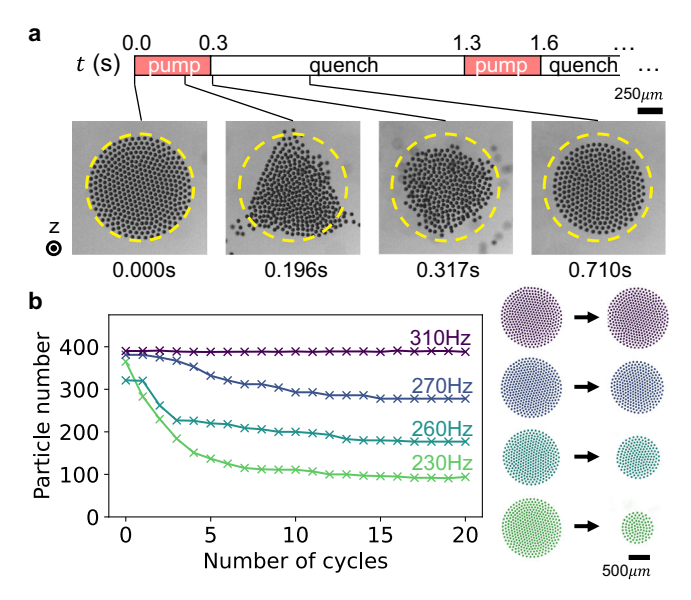


Fig. 5 | **Controlling the size of an acoustically levitated granular raft. a** A levitated raft being pumped to undergo shape oscillations to shed particles, before being quenched and stabilized with fewer particles. The yellow dashed circle has the same size in each image and serves as a visual guide. **b** Evolution under repeated pump-quench cycling of the number of particles in a raft for different pump frequencies. Images to the right of the plot show the initial and final raft configuration, demonstrating the ability to control the raft size.

properties or geometries, and it can be generalized to control structures when multiple stable configurations are available, as long as the resonances for activated states and targeted absorbing states are sufficiently well separated in the pumping state diagram.

As our method only depends on a suitable spectrum of excitable vibration modes, we expect it can be applied to a wide range of systems with tunable interactions beyond acoustically levitated ones. both reciprocal and non-reciprocal, including dielectric and magnetic particles^{36,37}, as well as optically trapped particles^{7,38,39}. For example, used for directed self-assembly, it might offer a versatile way to selectively eliminate undesired sub-structures early on, before they seed the subsequent assembly into larger dysfunctional configurations. Since our approach focuses on manipulating the interactions of particles in close proximity, we expect that it can be integrated with far-field methods, which can generate reconfigurable or steerable potential gradients over larger length scales. For example, using farfield-based methods9,11 to generate an array of acoustic potential wells, and seeding each with multiple particles, parametric pumping of these wells could then be applied to generate many copies of the targeted particle configuration simultaneously. Finally, extensions might adapt parametric pumping for controlling the assembly of micro-robots¹⁶, non-contact cell counting⁴⁷, and manipulation of defects in colloidal crystals and liquid crystals^{48,49}.

Methods

Acoustic levitation experiments

We use a single-axis ultrasound transducer to levitate particles, as shown in Fig. 2a. An aluminum horn is attached to a stack of piezo elements, which is driven by a signal generator (Keysight, EDU33212A) and an amplifier (AA Lab Systems, A-301 HS). The bottom of the horn is positioned half a sound wavelength above a transparent reflector plate to generate a standing wave. Both the horn and the reflector are grounded to minimize particle charging.

Two high-speed cameras capture the bottom and side views of the levitated particles. To improve image quality, we used backlighting: Light from one source, angled upward, is reflected from the white-

painted bottom surface of the horn, enabling us to capture high-resolution bottom-view images with camera 1 (Phantom T1340) through a mirror angled at 45 degrees. Camera 1 is equipped with a Nikon ED AF Micro Nikkor 200 mm lens to capture the dynamics of the levitated 5-particle system, and with a Navitar Resolv4K lens (working distance 72 mm) for imaging the levitated 2-particle system and the larger rafts. A second light source illuminates from the left, enabling us to simultaneously capture side-view images with camera 2 (Phantom, VEO1010S, equipped with a Nikon AF Micro Nikkor 70–180 mm lens).

A temperature controller (Conductus, LTC-20) stabilizes the horn temperature within 50 mK and minimizes any temperature-dependent drift in acoustic power. An acrylic enclosure thermally isolates the setup from the ambient conditions in the lab, further improving temperature control. An interferometric pressure sensor (XARION Laser Acoustics, Eta100 Ultra) is positioned next to the acoustic cavity to measure the real-time sound pressure. Before each experiment, an X-ray de-ionizer (Hamamatsu, L9491) is turned on for 10 seconds to neutralize the electric charge on the levitated particles.

We use polystyrene spheres with diameter $D = (41.1 \pm 0.5) \, \mu m$ (microParticles GmbH). Before being placed into the acoustic trap, these particles are coated with a layer of nanoparticles (Evonik Aeroxide AluC) to minimize sticking due to van der Waals interaction.

Finite-element analysis and calculation of the stiffness matrix

We use the FEM solver COMSOL Multiphysics to carry out simulations of vibrational modes, taking into account particle interactions due to scattered sound as well as sound-induced microstreaming. The simulation domain is a cylinder with diameter 10 mm and height 4.94 mm, corresponding to half of the ultrasound wavelength λ . The particles are placed on the nodal plane in the center of this cylinder. The simulation proceeds in two steps. The first step is a thermoviscous acoustics calculation in the frequency domain, where the top of the cylinder is set to oscillate in the vertical, z-direction, and the bottom is fixed. To mimic the open side of the acoustic cavity, the side wall of the cylinder is set to have a slip boundary condition. The surfaces of levitated particles are set to no-slip boundary conditions. A second step is a laminar flow calculation, carried out to obtain the time-averaged streaming flow between particles. Forces acting on each particle are calculated by integrating the viscous stress and pressure on the particle surface.

The stiffness matrix, K, for each configuration can then be constructed by simulations in which each individual particle is slightly displaced from its stable, steady-state position. K_{ii} represents the linear response of the system in direction of j-th degree of freedom (DoF) when a displacement occurs in the direction of the i-th DoF, with $1 \le i, j \le 15$. To calculate this response, we displace the particle along the direction of the i-th DoF across a distance from +0.5 D to -0.5 D using a total of 11 simulations with the smallest displacement of 0.01 D near the stable position and conduct a polynomial fit of the resulting force acting in the direction of the j-th DoF as a function of the displacement (to third order). K_{ij} is then given by the linear term of this fit. Matlab is used to vary the displacement of particles in all simulations. This method does not assume pairwise or reciprocal interactions and, therefore, is suitable for analyzing the linear response of the system regardless of the nature of the interactions. A reduced-order model could be used to reduce the complexity of the stiffness matrix calculation. Order reduction can be done by considering the symmetry of the system (such as permutation symmetry in the pentagon state, reported in the main text), or by focusing only on the relevant vibrational modes achievable in the experiments (such as adapting a continuum model that represents the granular rafts reported in the main text as homogeneous materials with effective material properties). Another useful way of locating the vibrational frequencies in our system, as well as in other possible systems, is conducting a frequency sweep experimentally. Specifically, by applying parametric pumping to

the system with a small modulating depth and a small modulating time while sweeping through different frequencies, one can observe the growth rate of vibrational modes for different structures without destroying them, and then one can use this information to determine the best combination of parameters to select structures of interest.

Calculation of the mode growth rate γ

For an ensemble of particles with generalized coordinates **x**, inertial matrix **M** and stiffness matrix **K**, its equation of motion is

$$\mathbf{M}\frac{d^2\mathbf{x}}{dt^2} + \gamma_d \frac{d\mathbf{x}}{dt} + \mathbf{K}\mathbf{x} = \mathbf{0},\tag{2}$$

when subject to linear damping with damping coefficient γ_d . Under acoustic parametric pumping, Eq. (1), the equation of motion becomes

$$\mathbf{M}\frac{d^2\mathbf{x}}{dt^2} + \gamma_d \frac{d\mathbf{x}}{dt} + \mathbf{K}(1 + \varepsilon_{\text{am}} \sin(2\pi f_{\text{am}}t))^2 \mathbf{x} = \mathbf{0}.$$
 (3)

By simultaneously diagonalizing **M** and **K** we can separate different VMs. For each VM with eigenfrequency ω_i and eigenvector \mathbf{x}_i , we assume a solution of the form $\mathbf{x} = \eta_i(t)\mathbf{x}_i$. The equation then becomes

$$\left(\frac{d^2}{dt^2} + \gamma_d \frac{d}{dt} + \omega_i^2 ((1 + \varepsilon_{\text{am}} \sin(2\pi f_{\text{am}} t))^2\right) \eta_i(t) = 0, \tag{4}$$

which is integrated numerically (scipy.integrate.odeint). The function $\eta_i(t)$ oscillates as a function of time t, and its amplitude will exponentially increase or decrease. Thus, an exponential fit can be made using the peaks of $\eta_i(t)$, giving the mode's growth rate γ_i .

In the two simulated systems, the rod-plus-spheres cluster and the 3D LJ sphere cluster, the interaction strength can be modulated directly, so the equation is

$$\left(\frac{d^2}{dt^2} + \gamma_d \frac{d}{dt} + \omega_i^2 \left(1 + \varepsilon_{\text{am}} \sin(2\pi f_{\text{am}} t)\right) \eta_i(t) = 0,$$
 (5)

and we can extract γ_i in the same manner as described above. Finally, to obtain the normalized growth rates plotted in the parametric pumping state diagrams, we divide the damping-free growth rate γ_i which is found by solving the equation of motion for the case of $\gamma_d = 0$, by the damping rate γ_d .

Interactions for the rod-plus-spheres cluster

In this particular example, we do not consider the multibody and non-reciprocal nature of acoustic interactions and instead focus on particle shape. Therefore, for the interactions between all spheres in this system, including the three spheres making up the rod, we take a generalized Lennard-Jones potential⁵⁰,

$$E = \frac{E_0}{n - m} \left[m \left(\frac{r_0}{r} \right)^n - n \left(\frac{r_0}{r} \right)^m \right]. \tag{6}$$

We choose m=3 to mimic the attractive acoustic scattering forces in the experiment that scale with r^{-4} , and choose n=6 to provide a short-range repulsive interaction that mimics microstreaming. E_0 is set to 10 nJ so that the interaction strength is similar to that in the experiment. The three stable states have potential energies -79.4 nJ, -73.2 nJ, and -72.1 nJ. A weak confining force is applied to all particles to bring them back together during the quenching step of a cycle. The molecular dynamics simulation is carried out using LAMMPS⁵¹ with damping coefficient 6.28×10^{-6} kg s⁻¹ and timestep 5×10^{-8} s.

Markov models

The Markov model for the levitated five-particle experiment is built with transition matrices shown in Supplementary Fig. 4a, where the numbers are determined from experimental observations after the quenching step, and are based on the assumption that pumping will always bring a base state into the unstable state. This model qualitatively captures the observed rapid absorption. However, in the experiments, there can be a weak history dependence because sometimes the particles retain oscillations due to non-conservative interactions for a longer time than the quenching period. This is not captured by the Markov model and is likely to contribute to the quantitative difference we see in Fig. 3h between measured data and prediction.

Absorbing Markov models for the rod-plus-spheres cluster are built with transition matrices shown in Supplementary Fig. 4b, c. These matrices refer to the cases when the system is pumped with different parameters marked in Fig. 4a. For example, the first matrix with the red cross sign on the top shows the transition rate between three states, red (r), green (g), and blue (b), for the case that the system is pumped using the parameters marked by the red cross. Under this procedure. the green and blue states are stable, but the red state has a non-zero possibility of transition. The numbers in the matrices are obtained from simulating one pump-quench cycle with 10,000 random initial conditions for each set of parameters. Supplementary Fig. 4d shows the transition matrix for the case that the system is successively pumped with two sets of parameters, i.e., the first method mentioned in the main text. As an example, the first transition matrix corresponds to the system being first pumped using blue cross parameters, quenched, pumped using the green cross parameters, and then quenched again. The result is identical to that obtained by multiplying the two matrices corresponding to the two crosses. Supplementary Fig. 4e, f gives the expected quenching steps needed by absorption into the desired state, calculated from the transition matrices in Supplementary Fig. 4c, d.

Data availability

The data that support the findings of this study have been deposited in the Materials Data Facility database⁵².

Code availability

The code that supports the findings of this study has been deposited in the Materials Data Facility database⁵².

References

- Melde, K., Mark, A. G., Qiu, T. & Fischer, P. Holograms for acoustics. Nature 537, 518–522 (2016).
- Ozcelik, A. et al. Acoustic tweezers for the life sciences. Nat. Methods 15, 1021–1028 (2018).
- Yang, S. et al. Harmonic acoustics for dynamic and selective particle manipulation. *Nat. Mater.* 21, 540–546 (2022).
- Lim, M. X., VanSaders, B. & Jaeger, H. M. Acoustic manipulation of multi-body structures and dynamics. *Rep. Prog. Phys.* 87, 064601 (2024).
- Grier, D. G. A revolution in optical manipulation. Nature 424, 810–816 (2003).
- Maragò, O. M., Jones, P. H., Gucciardi, P. G., Volpe, G. & Ferrari, A. C. Optical trapping and manipulation of nanostructures. *Nat. Nanotechnol.* 8, 807–819 (2013).
- Gong, Z., Pan, Y.-L., Videen, G. & Wang, C. Optical trapping and manipulation of single particles in air: principles, technical details, and applications. J. Quant. Spectrosc. Radiat. Transf. 214, 94–119 (2018).
- Yang, Y., Ren, Y., Chen, M., Arita, Y. & Rosales-Guzmán, C. Optical trapping with structured light: a review. Adv. Photonics 3, 034001 (2021).

- Caleap, M. & Drinkwater, B. W. Acoustically trapped colloidal crystals that are reconfigurable in real time. *Proc. Natl. Acad. Sci.* 111, 6226–6230 (2014).
- Hirayama, R., Martinez Plasencia, D., Masuda, N. & Subramanian, S. A volumetric display for visual, tactile and audio presentation using acoustic trapping. *Nature* 575, 320–323 (2019).
- Marzo, A. & Drinkwater, B. W. Holographic acoustic tweezers. Proc. Natl. Acad. Sci. 116, 84–89 (2019).
- Snezhko, A. & Aranson, I. S. Magnetic manipulation of selfassembled colloidal asters. *Nat. Mater.* 10, 698–703 (2011).
- Yan, J., Bloom, M., Bae, S. C., Luijten, E. & Granick, S. Linking synchronization to self-assembly using magnetic janus colloids. *Nature* 491, 578–581 (2012).
- Edwards, T. D. & Bevan, M. A. Controlling colloidal particles with electric fields. *Langmuir* 30, 10793–10803 (2014).
- Mehdizadeh Taheri, S. et al. Self-assembly of smallest magnetic particles. Proc. Natl. Acad. Sci. 112, 14484–14489 (2015).
- Deng, Y. et al. Fabrication of magnetic microrobots by assembly. Adv. Intell. Syst. 6, 2300471 (2024).
- 17. Zhang, Z. & Glotzer, S. C. Self-assembly of patchy particles. *Nano Lett.* **4**, 1407–1413 (2004).
- Feng, L., Dreyfus, R., Sha, R., Seeman, N. C. & Chaikin, P. M. Dna patchy particles. Adv. Mater. 25, 2779–2783 (2013).
- Sacanna, S. et al. Shaping colloids for self-assembly. Nat. Commun. 4, 1688 (2013).
- Valignat, M.-P., Theodoly, O., Crocker, J. C., Russel, W. B. & Chaikin, P. M. Reversible self-assembly and directed assembly of dna-linked micrometer-sized colloids. *Proc. Natl. Acad. Sci.* 102, 4225–4229 (2005).
- Chakraborty, I. et al. Self-assembly dynamics of reconfigurable colloidal molecules. ACS Nano 16, 2471–2480 (2022).
- Evans, C. G., O'Brien, J., Winfree, E. & Murugan, A. Pattern recognition in the nucleation kinetics of non-equilibrium self-assembly. Nature 625, 500–507 (2024).
- Nguyen, M. & Vaikuntanathan, S. Design principles for none-quilibrium self-assembly. *Proc. Natl. Acad. Sci.* 113, 14231–14236 (2016).
- Chvykov, P. et al. Low rattling: a predictive principle for selforganization in active collectives. Science 371, 90–95 (2021).
- N. McDonald, M., Zhu, Q., F. Paxton, W., K. Peterson, C. & R. Tree, D. Active control of equilibrium, near-equilibrium, and far-fromequilibrium colloidal systems. Soft Matter 19, 1675–1694 (2023).
- Tang, X. et al. Optimal feedback controlled assembly of perfect crystals. ACS Nano 10, 6791–6798 (2016).
- Meng, G., Arkus, N., Brenner, M. P. & Manoharan, V. N. The freeenergy landscape of clusters of attractive hard spheres. *Science* 327, 560–563 (2010).
- Phillips, C. L. et al. Digital colloids: reconfigurable clusters as high information density elements. Soft Matter 10, 7468–7479 (2014).
- Perry, R. W., Holmes-Cerfon, M. C., Brenner, M. P. & Manoharan, V. N. Two-dimensional clusters of colloidal spheres: Ground states, excited states, and structural rearrangements. *Phys. Rev. Lett.* 114, 228301 (2015).
- Lim, M. X., Souslov, A., Vitelli, V. & Jaeger, H. M. Cluster formation by acoustic forces and active fluctuations in levitated granular matter. *Nat. Phys.* 15, 460–464 (2019).
- Boccardo, F. & Pierre-Louis, O. Controlling the shape of small clusters with and without macroscopic fields. *Phys. Rev. Lett.* 128, 256102 (2022).
- Brandenbourger, M., Locsin, X., Lerner, E. & Coulais, C. Non-reciprocal robotic metamaterials. *Nat. Commun.* 10, 4608 (2019).
- 33. Scheibner, C. et al. Odd elasticity. Nat. Phys. 16, 475-480 (2020).

- 34. Wu, B., VanSaders, B., Lim, M. X. & Jaeger, H. M. Hydrodynamic coupling melts acoustically levitated crystalline rafts. *Proc. Natl. Acad. Sci.* **120**, e2301625120 (2023).
- 35. Happer, W. Optical pumping. Rev. Mod. Phys. 44, 169 (1972).
- 36. Han, K. et al. Reconfigurable structure and tunable transport in synchronized active spinner materials. *Sci. Adv.* **6**, eaaz8535 (2020).
- 37. Yakovlev, E. V. et al. 2D colloids in rotating electric fields: a laboratory of strong tunable three-body interactions. *J. Colloid Interface Sci.* **608**, 564–574 (2022).
- Vijayan, J. et al. Cavity-mediated long-range interactions in levitated optomechanics. Nat. Phys. 20, 859–864 (2024).
- Reisenbauer, M. et al. Non-hermitian dynamics and non-reciprocity of optically coupled nanoparticles. Nat. Phys. 20, 1629–1635 (2024).
- 40. Kac, M. Can one hear the shape of a drum? The American Mathematical Monthly. Vol. 73, 1–23 (1966).
- 41. Gordon, C., Webb, D. & Wolpert, S. Isospectral plane domains and surfaces via Riemannian orbifolds. *Invent. Math.* **110**, 1–22 (1992).
- 42. Shen, C. L., Xie, W. J. & Wei, B. Parametrically excited sectorial oscillation of liquid drops floating in ultrasound. *Phys. Rev. E* 81, 046305 (2010).
- Dolev, A., Davis, S. & Bucher, I. Noncontact dynamic oscillations of acoustically levitated particles by parametric excitation. *Phys. Rev.* Appl. 12, 034031 (2019).
- 44. Wang, Y., Luo, L., Ke, M. & Liu, Z. Acoustic subwavelength manipulation of particles with a quasiperiodic plate. *Phys. Rev. Appl.* 17, 014026 (2022).
- 45. Arscott, F. M. Periodic differential equations: an introduction to Mathieu, Lamé, and allied functions (Elsevier, 2014).
- Silva, G. T. & Bruus, H. Acoustic interaction forces between small particles in an ideal fluid. *Phys. Rev. E* 90, 063007 (2014).
- 47. Picot, J., Guerin, C. L., Le Van Kim, C. & Boulanger, C. M. Flow cytometry: retrospective, fundamentals and recent instrumentation. *Cytotechnology* **64**, 109–130 (2012).
- Sandford O'Neill, J. J., Salter, P. S., Booth, M. J., Elston, S. J. & Morris, S. M. Electrically-tunable positioning of topological defects in liquid crystals. *Nat. Commun.* 11, 2203 (2020).
- Menath, J. et al. Acoustic crystallization of 2D colloidal crystals. Adv. Mater. 35, 2206593 (2023).
- Clarke, J. H. R., Smith, W. & Woodcock, L. V. Short range effective potentials for ionic fluids. J. Chem. Phys. 84, 2290–2294 (1986).
- 51. Thompson, A. P. et al. Lammps a flexible simulation tool for particle-based materials modeling at the atomic, meso, and continuum scales. *Comput. Phys. Commun.* **271**, 108171 (2022).
- 52. Mao, Q., Wu, B., VanSaders, B. & Jaeger, H. M. Dataset: structural reconfiguration of interacting multi-particle systems through parametric pumping. Available online at https://doi.org/10.18126/q7rx-9597. (2025).

Acknowledgements

We thank Nina Brown, Tali Khain, and Tom Witten for insightful discussions. This research was supported by the National Science Foundation through award number DMR-2104733. The work utilized the shared experimental facilities at the University of Chicago MRSEC, which is funded by the National Science Foundation under award number DMR-2011854. The research also benefited from computational resources and services supported by the Research Computing Center at the University of Chicago.

Author contributions

Q.M., B.W., B.V. and H.M.J. conceived the study. Q.M. performed the experiments and simulations. All authors contributed to the analysis of the results and to the writing of the manuscript.

Competing interests

The authors declare no competing interests.

Additional information

Supplementary information The online version contains supplementary material available at https://doi.org/10.1038/s41467-025-59631-3.

Correspondence and requests for materials should be addressed to Qinghao Mao.

Peer review information *Nature Communications* thanks the anonymous reviewers for their contribution to the peer review of this work. A peer review file is available.

Reprints and permissions information is available at http://www.nature.com/reprints

Publisher's note Springer Nature remains neutral with regard to jurisdictional claims in published maps and institutional affiliations.

Open Access This article is licensed under a Creative Commons Attribution-NonCommercial-NoDerivatives 4.0 International License, which permits any non-commercial use, sharing, distribution and reproduction in any medium or format, as long as you give appropriate credit to the original author(s) and the source, provide a link to the Creative Commons licence, and indicate if you modified the licensed material. You do not have permission under this licence to share adapted material derived from this article or parts of it. The images or other third party material in this article are included in the article's Creative Commons licence, unless indicated otherwise in a credit line to the material. If material is not included in the article's Creative Commons licence and your intended use is not permitted by statutory regulation or exceeds the permitted use, you will need to obtain permission directly from the copyright holder. To view a copy of this licence, visit http://creativecommons.org/licenses/by-nc-nd/4.0/.

© The Author(s) 2025